DOI: 10.21776/ub.jpacr.2018.007.02.406 *J. Pure App. Chem. Res.*, **2018**, 7(2), 257-265
10 September 2018

Synthesis and Modification of Macroporous Titania using Silver Nanoparticles

Natalita Maulani Nursam,[1,2,*] Jeannie Ziang Yie Tan[2,3]

[1]Research Center for Electronics and Telecommunication, Indonesian Institute of Science
Komplek LIPI Gedung 20 lantai 4, Jl Sangkuriang Cisitu, Bandung 40135, Indonesia
[2]Particulate Fluids Processing Centre, School of Chemistry, the University of Melbourne, Melbourne, Victoria 3010, Australia
[3]Institute of Mechanical, Process & Energy Engineering, Heriot-Watt University, Edinburgh, Scotland, United Kingdom.

[*]Corresponding email: natalita.maulani.nursam@lipi.go.id

Received 8 January 2018; Revised 20 July 2018; Accepted 20 July 2018

ABSTRACT

A synthesis method for preparing macroporous nitrogen and silver-modified titania via sol-gel route is presented. The addition of nitrogen and silver nanoparticles was carried out simultaneously with a hard templating technique using silica spheres packed into a three-dimensional opal structure. The influence of such modifications on the optical and chemical properties of titania was evaluated using photocatalytic degradation under visible light. The macroporous opal templated samples in this work performed better than the commercial titania, Degussa P25. The highest photocatalytic enhancement, showing more than eight times higher activity than the non-modified titania, was achieved by the opal templated sample prepared with 1.0 mol % of silver. Although silver addition and macroporous templating enhanced the visible light activity, the most significant improvement was afforded by the utilization of the silica opal template that gave rise to the high surface area (>100 m^2 g^{-1}) and promoted the surface charge interaction.

Key word: inverse opal, macroporous, photocatalysis, silver, titania.

INTRODUCTION

The inverse opal structure possesses unique optical characteristics, thus making it applicable for a wide range of applications such as photovoltaics [1], Li-ion batteries [2], sensing [3], optical waveguide [4], and photocatalysis [5-8]. The definition of the inverse opal is self-explanatory, referring to a structure made by the inverse replica of opal. Photonic crystal templates, such as colloidal silica, poly(methyl methacrylate) (PMMA) or polystyrene spheres, are the so-called opals, which are typically used as sacrificial templates to generate the inverse opal structure. Titania with an inverse opal (IO) macroporous structure has been demonstrated as a high-performance photocatalyst material, owing to its high porosity and large surface area, hence allowing easy adsorption and mass transport for organic pollutants or other substances to reach the active sites on the titania surface.

In order to further improve the photocatalytic performance of titania, including those with IO forms, many attempts have been made to modify the intrinsic structure. This is mostly targeted at reducing the recombination of the photoexcited electron-hole, and expanding the spectral response of titania toward the visible light range. Modifications via

The journal homepage www.jpacr.ub.ac.id
p-ISSN : 2302 – 4690 | e-ISSN : 2541 – 0733

chemical doping have been one of the common and convenient methods used to achieve these purposes. Doping with metal ions [9] or nonmetal elements [10] has been reported to improve the visible light activity primarily due to the impurities introducing new energy states in the titania bandgap. Single doping or metal nanoparticle loading on IO titania has been fairly well reported in the literature, but to a far lesser extent compared to titania nanoparticles. The incorporation of noble metal nanoparticles, such as Au [11] or Pt [12] into IO titania has been the most common strategy to increase the electron transfer for visible light photocatalysis or water splitting [13]. For example, Chen et. al. [5] filled the interstices of polystyrene opals on a Ti substrate with a Pt layer through electrochemical deposition followed by coating with titania precursor. This Pt/IO titania material exhibited a rate constant up to 3 orders of magnitude higher compared to the similar film made of titania nanoparticles without the IO structure. Dinh et. al. [14] fabricated IO titania by anchoring Au nanoparticles into colloidal silica via a layer-by-layer technique, followed by the deposition of titanate nanodisks as the outer thin walls. Meanwhile, Wang et. al. [15] reported the doping of nitrogen into an IO titania monolith prepared using PMMA and ethanediamine, showing an enhanced photocatalytic activity both under visible and solar irradiation. Unlike research into single doping or metal nanoparticle loading on IO titania, applications of co-modification on titania with IO structure have been rarely explored, possibly due to the complications generated by the multiple effects of morphological structuring and modification of properties.

In this work, multiple strategies were applied simultaneously in designing titania materials to obtain a photocatalyst with a superior photocatalytic activity. Herein, porous titania was loaded with silver nanoparticles (Ag-TiO_2), aiming to reduce the electron-hole recombination through the formation of a Schottky barrier at the silver-titania interface [5]. Meanwhile, a hard templating method was also used to make a macroporous inverse opal structure. The impact of each strategy for enhancing the photocatalytic activity was evaluated by measuring the photodegradation of aqueous methylene blue (MB) under visible light.

EXPERIMENT

Materials

Titanium (IV) butoxide (TBT, 97%) and tetraethyl orthosilicate (TEOS, 98%) were purchased from Sigma-Aldrich. Ethanol (EtOH) and sodium hydroxide (NaOH) pellets were supplied by Merck. Ammonia (NH_4OH, 30%), nitric acid (HNO_3, 70%) and silver nitrate ($AgNO_3$, 99.5%) were obtained from Chem-Supply, Adelaide Australia. Methylene blue (MB) was purchased from BDH Chemicals, Ltd., Poole England. Water obtained from a reverse osmosis system was used throughout the experiment. All chemicals were reagent grade and used as received.

Materials Preparation

Synthesis of colloidal silica

The silica templates used in this thesis were prepared following the Stöber method [16]. First, a mixture of EtOH (750 mL), water (60 mL), and ammonia (40 mL) was magnetically stirred. After 5 min, TEOS (45 mL) was added and stirring was continued for another 4 h. The formed silica spheres were separated from the solution by centrifugation followed by washing repeatedly in EtOH. To obtain the 3D assembly of closely packed silica spheres, the precipitates were re-dispersed in water followed by sonication and centrifugation at 2000 rpm for 10 h. The separated pellets were then dried overnight at 60 °C to improve the necking between the spheres. The dried silica monoliths had an iridescent reflection as the result of optical diffraction by the opals.

Preparation of titania nanoparticles (NP)

To prepare the precursors for pristine titania and Ag-TiO_2, 9 mL of TBT was mixed with 33 mL of EtOH by magnetically stirring for 30 min. A solution of 0.5 mL of water and 5 mL of EtOH was mixed and then added dropwise into the TBT/EtOH (for non-doped TiO_2). To prepare the silver ion doped titania, 4.2, 21 and 42 mg of $AgNO_3$ (corresponding to concentrations of 0.1, 0.5 and 1.0 mol %) was dissolved in the water/EtOH solution for 30 min before being added dropwise to the alkoxide solution. Stirring was continued for another 2 h in a closed beaker. The non-doped TiO_2 and Ag-TiO_2 solutions were then aged in an oven at 60 °C for 24 h, followed by centrifugation to collect the precipitate, which was then dried at 60 °C for 3 days.

Preparation of titania inverse opal (IO)

To prepare the IO Ag-TiO_2, the water component of the water/EtOH solution was replaced by 1 M HNO_3 as a stabilizer to prevent the precipitation of titania. All other materials and procedures remained the same as in the preparation of the NP samples.

A typical literature method was used for preparing the IO titania structure [17]. First, a filter paper (Whatman® qualitative, Grade 1 90 mm in diameter) was placed in a porcelain Buchner funnel as part of a standard filtration setup. To prepare the template, 5 g of dried silica bead monoliths were slightly crushed with a metal spatula to give fractured pieces of no more than 3 mm on a side. The crushed silica was then spread evenly on the filter paper (pre-wetted with EtOH), followed by dropwise addition of titania precursor. The numeric ratio of template and titania precursor was equal; for example, 5 mL of titania precursor was used for 5 g of silica. The funnel was then covered with Parafilm M® while a strong vacuum suction (0.8-1.0 bar) was applied for approximately 30 s to draw the precursor solutions through the silica and fill the interstices between the closely packed silica. The silica/titania composites were then collected and dried in an oven at 60 °C for 20 h.

Thermal treatment

All samples were calcined at 450 °C for 1 h with a ramping rate of 3 °C per min in a muffle furnace (Labec). After calcination, the silica template in all IO samples was removed by treating the samples in 2 M NaOH at 80 °C for 2 h. The undissolved particles were removed by centrifugation (Allegra® 64R, Beckman Coulter, Inc. with the fixed-angle rotor) and then rinsed with water several times to remove any possible impurities from the treatment.

The final materials were divided into two groups. The first group, consisting of non-templated nanoparticle composites, were labeled as NP Ti-Ag x %, where x was the molar concentration of silver added during the sol−gel synthesis. Likewise, samples prepared with silica opal templating in the second group were named as IO Ti-Ag x %.

Characterizations

The morphology of the samples was analyzed using scanning electron microscopy (SEM, FEI Quanta 400F, USA) dan transmission electron microscopy (TEM, FEI Tecnai F20, USA). X-ray diffraction (XRD) analysis was carried out using Bruker D8 diffractometer with Cu Kα radiation. Pore size and surface area analysis were performed using gas sorption technique with Micromeritics Tristar II instrument, wherein samples were degassed at 150 ˚C at 100 mTorr for a minimum of 6 h prior to the measurements.

Photocatalytic Activity Evaluation

Photodecomposition of methylene blue was carried out to evaluate the photocatalytic activity of the samples under visible light (420 – 650 nm). The reactor consisted of water-jacketed glass beaker placed under 500 W of Xe-Hg lamp (Oriel), wherein 50 mg of ground samples were dispersed in 50 mL of aqueous methylene blue (25 ppm) and stirred throughout the reaction. The aliquots were collected at the specific time interval and the absorbance was measured using FlexStation 3 Kinetic Plate Reader. The apparent reaction rate constant, k_{app}, was calculated from the slope of $ln[C(t)/C_0]$ versus t, where C_0 and $C(t)$ is the initial concentration and concentration measured after t min of irradiation, respectively.

RESULTS AND DISCUSSION

Herein, the Stöber method was selected to produce the silica spheres, as it provides straightforward size control that is typically achieved by tuning the ammonia/TEOS ratio during the synthesis [16]. The schematic of the inverse opal titania composite formation is shown in Figure 1. Infiltration of a preformed colloidal crystal template with a sol−gel titania precursor was carried out to produce various IO titania composites; capillary force infiltration of the colloidal silica was assisted by vacuum infiltration to draw the precursor through the silica. To obtain a porous titania structure, the silica was dissolved by treating the silica/titania hybrids in a heated NaOH solution. Dissolving in alkaline solution was selected as a milder alternative to the highly corrosive hydrofluoric acid solution that is typically used in the literature [18-19].

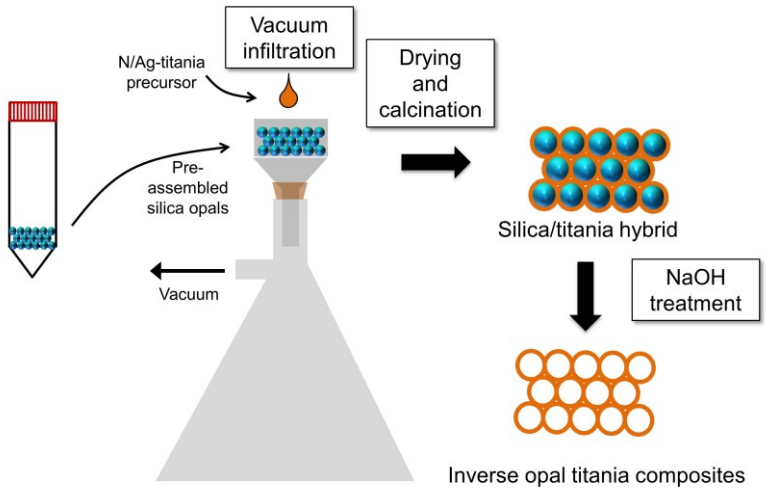

Figure 1. Schematic of the method used to prepare inverse opal samples.

Figure 2a and 2b show that the diameter of the silica spheres was in the narrow range of 420-440 nm. Figure 2a also showed that the size of the silica beads was relatively monodisperse. SEM images obtained from representative non-templated NP samples indicated that in the absence of a template macropores were not observed (see Figure 2c). The morphology of the IO titania after the removal of silica is shown in Figure 2d. Spherical voids were formed after template removal, replicating the shape and size of the silica spheres in the template scaffold, but without destroying either the pore structure or the titania walls. The macropore diameter was similar to the original size of the silica beads (i.e. 390 to 420 nm), suggesting that there was no significant shrinkage during the calcination step. The low-

resolution SEM image shown in Figure 2d shows that IO titania had disordered open pores instead of a continuous long-range ordered structure. Insufficient necking between the silica spheres that led to the loosely packed opals likely caused this. A few areas comprising thick walls or dense nanoparticles were found in all IO samples, indicating areas in which there was no silica template while they have filled initially with titania precursor. This could be formed by the excessive liquid precursor that was not withdrawn by the vacuum during the infiltration. It was confirmed that the addition of silver NPs did not alter the IO titania structure. TEM images in Figure 3a show the porous structure of the IO Ti-Ag-1.0 % particles as the result of silica templating. These TEM images also illustrate that the macropores were closely interconnected and had relatively uniform pore size. The addition of silver did not disrupt the integrity of the macroporous structure. The presence of silver, appearing as black spots, was confirmed by the HRTEM image in Figure 3b, which also indicated that silver nanoparticles were randomly distributed within the spherical aggregates of the titania matrix. Further identification using HRTEM clearly distinguished between particles within the composites. The presence of silver was confirmed based on the lattice fringes with *d*-spacing values of approximately 0.22 and 0.35 nm, corresponding to silver and the (101) plane of anatase titania, respectively.

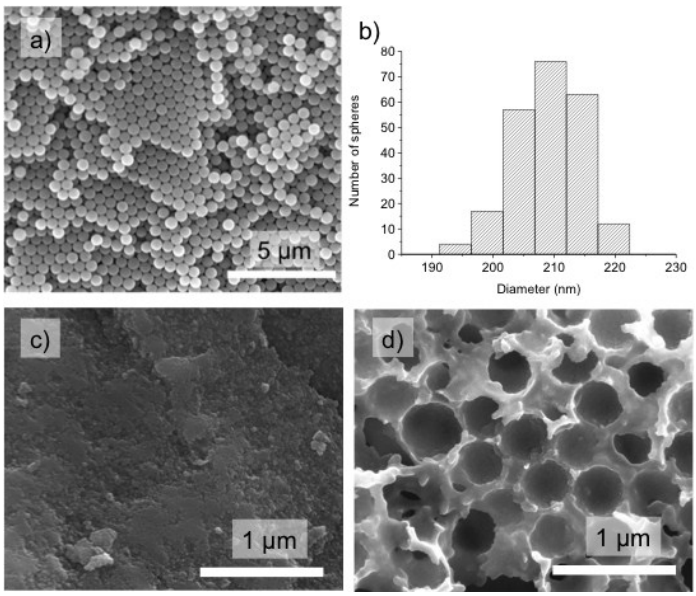

Figure 2. a) SEM image of silica synthesized using Stober method, b) size distributions of the silica beads, c) SEM image of non-templated TiO_2, and d) SEM image of IO-TiO_2.

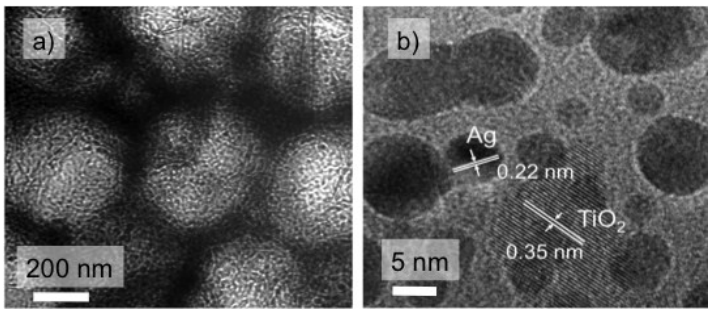

Figure 3. a) TEM image of IO Ti-Ag-1.0 % and b) HRTEM image showing the lattice fringes of anatase TiO_2 and silver.

XRD analysis was utilized for two purposes. First, the XRD data was used to determine whether there was any possible residual silica after the NaOH treatment, and what influence the silica had on the crystal phase and size of the final IO titania materials. Figure 4a shows a broad peak between approximately 2θ ~15° and 40° for pure silica spheres calcined at 450 °C that corresponds to the amorphous phase. A similar peak was observed for the silica/titania hybrid, obstructing the detection of any possible crystalline peaks. After the template was etched away, peaks that were indexed to the titania anatase phase were clearly in evidence. However, it was noted that the main anatase peak of the IO sample exhibited a slightly unusual profile (i.e. the low intensity was broadly distributed), which might be attributed to the presence of amorphous silica remaining in the sample that is below the detection limit of XRD. Secondly, the XRD data was used to see the effect of silver concentration on the crystal phase of the composites. The XRD data shown in Table 1 indicated that all of the IO titania composites were exclusively anatase phase, which was consistent with the previous NP titania composites. According to the peak intensity and Scherrer calculation, the crystallinity and crystal sizes of the IO Ti-Ag-x samples group were lower than their non-templated counterparts, except when the initial Ag concentration was 1.0 mol %.

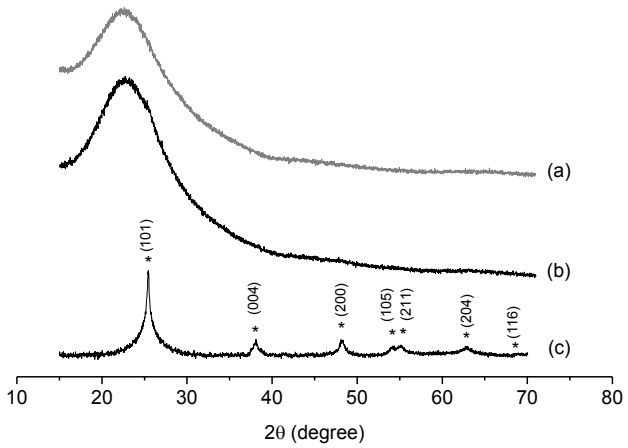

Figure 4. XRD patterns of (a) silica calcined at 450 °C, (b) silica/IO Ti-Ag-0.0 % hybrid before template removal and (c) IO Ti-Ag-0.0 % after template removal.

Table 1. Physical properties of the NP and IO titania composites obtained from XRD and gas sorption characterizations.

	Crystal phase		**Crystal diameter (nm)**		**BET surface area (m^2 g^{-1})**	
	NP	IO	NP	IO	NP	IO
Ti-Ag-0.0 %	anatase	anatase	21.1	15.2	23.6	21.4
Ti-Ag-0.1 %	anatase	anatase	21.1	14.4	37.8	194.8
Ti-Ag-0.5 %	anatase	anatase	16.4	14.2	58.3	363.3
Ti-Ag-1.0 %	anatase	anatase	16.2	16.6	6.4	19.5

With the exception of IO Ti-Ag-0.0 %, Table 1 shows that the IO templated samples possessed BET surface areas that were at least 2 times higher than their NP counterparts. The presence of large voids from the silica template led to more abundant pore volumes and accessible surface area, thus, higher surface area was obtained. Overall, the higher surface areas shown by most of the IO samples compared to the NP samples were well expected due to the smaller crystal size. However, since the crystal sizes of NP and IO Ti-Ag-1.0 % samples were comparable, the presence of residual silica in the IO samples was also suspected to contribute to the high surface area. The fact that NP Ti-Ag-0.0 % and IO Ti-Ag-0.0 % had similarly modest BET surface areas suggests that the crystal aggregation that led to larger mesopore size was also linked to the presence of silver nanoparticles. In the case of NP Ti-Ag-1.0 % and IO Ti-Ag-1.0 %, it was suspected that the low surface areas were caused by the large density of silver aggregates. This was supported by the fact that both samples had reasonably similar pore diameter (i.e. ~6.3 nm) and associated pore volumes (i.e. ~0.043 cm^3 g^{-1}) with the rest of NP Ti-Ag-x samples.

Figure 5 displays comparisons of the apparent rate constant, k_{app}, presented as the mean value from three replicate MB photodegradation tests under visible light (λ = 420-650 nm). All of the IO templated samples demonstrated enhanced visible light activity compared to the non-templated NP samples, and also had a higher k_{app} than P25 (k_{app} = 3.7 × 10^{-3} min^{-1}). The highest photocatalytic activity was produced by IO Ti-Ag-1.0 % with a mean k_{app} of 4.9 × 10^{-3} min^{-1}, which was almost three times higher than P25 and four times higher than the non-doped TiO_2, NP Ti-Ag-0.0 % (i.e. k_{app} = 1.2 × 10^{-3} min^{-1}).

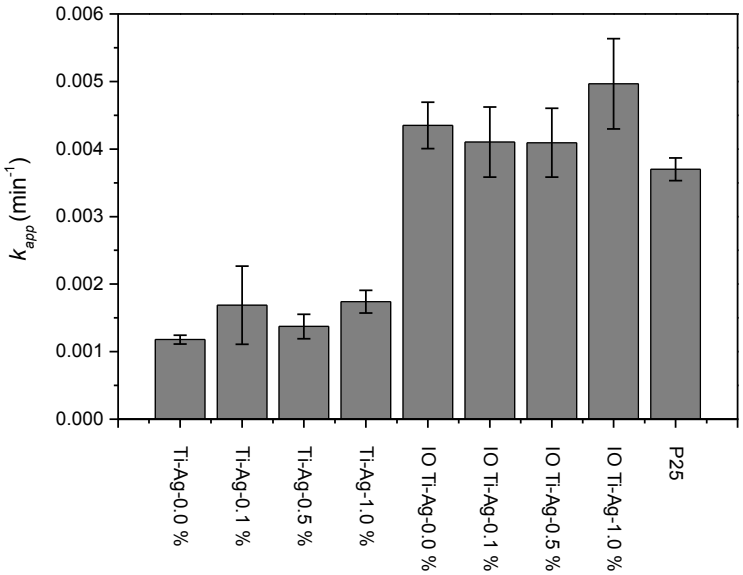

Figure 5. Apparent reaction rate constant (k_{app})

The addition of silver led to higher photocatalytic activity compared to the pristine titania, both with or without IO templating. The fermi level of silver is lower than the fermi level of titania, thus photoexcited electrons from the titania can be captured by the noble metal while the photoexcited holes remain in the valence band [20-22]. The highest visible light activity was shown by the samples prepared with 1.0 mol % of silver. While the enhancement factor varied depending on the doping quantity, the addition of silver enhanced the visible light activity of NP titania less than two-fold. When compared to P25, the resulting rate constants of all NP Ti-Ag-x composites showed a reduction in activity by more

than half. The overall results suggest that, despite providing moderate benefits in some cases, silver loading did not promote significant enhancement in the visible light activity. Similar enhancement factors were also obtained for the IO samples, which suggested that the IO structure was primarily responsible for the greatly improved visible light activity.

All of the IO samples showed considerably higher photocatalytic visible light activity compared to the NP samples. One parameter that sets the NP and IO samples apart was the specific surface area. Apart from IO Ti-Ag-0.0 % and IO Ti-Ag-1.0 %, the BET surface area of the IO Ti-Ag-x was at least five times higher compared to their corresponding NP samples (see Table 1). Apart from the two exceptions, the surface areas of the IO samples were also much higher than that of P25 (listed by the manufacturer as 50 m^2 g^{-1}). A large surface area in photocatalyst materials is well known to benefit the adsorption of pollutant molecules and accessibility towards surface active sites for photocatalytic reactions. Thus, the visible light activity of the IO titania samples was likely to have been promoted by their high surface areas as a consequence of the porous IO structure.

CONCLUSIONS

To optimize the visible light activity of the macroporous IO anatase titania, modifications with silver nanoparticles were carried out. The physicochemical properties of the titania composites were influenced by both silver loading and the use of colloidal crystal templating. The anatase crystal size decreased with the increase in silver content. The application of IO templating also reduced the crystal size and mostly caused a substantial increase in the surface area. The IO templated samples consistently showed superior performance compared to their NP counterparts. The highest photocatalytic activity was demonstrated by IO templated titania modified with silver NPs obtained from the highest initial silver content of 1.0 mol %. The enhanced activity was in part attributed to the surface area. In terms of the enhancement of visible light activity, the results of this study demonstrated the great potential of colloidal silica templating for producing macroporous anatase titania composites.

ACKNOWLEDGMENT

NMN acknowledged the Melbourne International Research Scholarship for the funding during the data collection of this work. The travel and publication funding was provided by the INSINAS research program 2017 from the Ministry of Research, Technology and Higher Education of the Republic of Indonesia contract no. 04/INS-2/PPK/E/E4/2017.

REFERENCES

[1] Lee, J. W., J. H. Moon, *Nanoscale,* **2015,** 7 (12), 5164-5168.
[2] Doherty, C. M., R. A. Caruso, B. M. Smarsly, C. J. Drummond, *Chem. Mater.,* **2009,** 21 (13), 2895-2903.
[3] Fenzl, C., S. Wilhelm, T. Hirsch, O. S. Wolfbeis, *ACS Appl. Mater. Interfaces,* **2013,** 5 (1), 173-178.
[4] Rinne, S. A., F. Garcia-Santamaria, P. V. Braun, *Nat. Photonics,* **2008,** 2 (1), 52-56.
[5] Chen, H. A., S. Chen, X. Quan, Y. B. Zhang, *Environ. Sci. Technol.,* **2010,** 44 (1), 451-455.
[6] Sordello, F., C. Duca, V. Maurino, C. Minero, *Chem. Commun.,* **2011,** 47 (21), 6147-6149.
[7] Xin, L., X. Liu, *RSC Adv.,* **2015,** 5 (88), 71547-71550.
[8] Stefan, S., T. Harun, *Eur. J. Inorg. Chem.,* **2018,** 2018 (20-21), 2350-2355.

[9] Anh Tuan, V., N. Quoc Tuan, B. Thi Hai Linh, T. Manh Cuong, D. Tuyet Phuong, T. Thi Kim Hoa, *Adv. Nat. Sci.: Nanosci. Nanotechnol.,* **2010,** 1 (1), 015009.
[10] Devi, L. G., R. Kavitha, *Appl. Catal., B,* **2013,** 140-141, 559-587.
[11] Kim, K., P. Thiyagarajan, H. J. Ahn, S. I. Kim, J. H. Jang, *Nanoscale,* **2013,** 5 (14), 6254-6260.
[12] Liu, J., G. L. Liu, M. Z. Li, W. Z. Shen, Z. Y. Liu, J. X. Wang, J. C. Zhao, L. Jiang, Y. L. Song, *Energy Environ. Sci.,* **2010,** 3 (10), 1503-1506.
[13] Schneider, J., M. Matsuoka, M. Takeuchi, J. L. Zhang, Y. Horiuchi, M. Anpo, D. W. Bahnemann, *Chem. Rev.,* **2014,** 114 (19), 9919-9986.
[14] Dinh, C. T., H. Yen, F. Kleitz, T. O. Do, *Angew. Chem. Int. Ed.,* **2014,** 53 (26), 6618-6623.
[15] Wang, T., X. Q. Yan, S. S. Zhao, B. Lin, C. Xue, G. D. Yang, S. J. Ding, B. L. Yang, C. S. Ma, G. Yang, G. R. Yang, *J. Mater. Chem. A,* **2014,** 2 (37), 15611-15619.
[16] Stober, W., A. Fink, E. Bohn, *J. Colloid Interface Sci.,* **1968,** 26 (1), 62-69.
[17] Holland, B. T., C. F. Blanford, A. Stein, *Science,* **1998,** 281 (5376), 538-540.
[18] Jiang, P., J. Cizeron, J. F. Bertone, V. L. Colvin, *J. Am. Chem. Soc.,* **1999,** 121 (34), 7957-7958.
[19] Johnson, S. A., P. J. Ollivier, T. E. Mallouk, *Science,* **1999,** 283 (5404), 963-965.
[20] Bumajdad, A., M. Madkour, *Phys. Chem. Chem. Phys.,* **2014,** 16 (16), 7146-7158.
[21] Enachi, M., M. Guix, T. Braniste, V. Postolache, V. Ciobanu, V. Ursaki, O. G. Schmidt, I. Tiginyanu, *Surf. Eng. Appl. Electrochem.,* **2015,** 51 (1), 3-8.
[22] Fei, T., Z. Rongshu, S. Kelin, O. Feng, C. Gang, *Environ. Eng. Sci.,* **2016,** 33 (3), 185-192.